Kingdom of Saudi Arabia
Imam Mohammad Ibn Saud Islamic University (IMSIU)
Faculty of Sciences – Department of Physics

;p

Geant4 Study of Proton Deflection in a Magnetic Field for Proton Therapy Beam Profiling

A graduation project submitted to the Department of Physics in partial fulfillment of the requirements for the degree of Bachelor of Science in Applied Physics

By

Hanan Aleidan

Luluah Al sabr

Razan Al mokhalfi

Supervisor

Dr Hanan Akhdar

IMSIU-Riyadh-KSA

May, 2025

Acknowledgements

الحمد لله الذي بنعمته تتم الصالحات، وبفضله وتوفيقه تم إنجاز هذا البحث العلمي. نسأل الله عز وجل أن يجعله عملاً خالصًا لوجهه الكريم، وأن ينفع به العلم وطلابه.

أتوجه بخالص الشكر وعظيم الامتنان إلى المشرفة دكتورة حنان أخضر على ما بذلته من جهد وتوجيه ودعم متواصل خلال فترة إعداد هذا البحث. لقد كان لتوجيهاتها السديدة وملاحظاتها القيمة الأثر الكبير في تطوير البحث وتحسينه.

كما أتقدم بجزيل الشكر والتقدير إلى أعضاء هيئة التدريس في كلية العلوم وتحديداً قسم الفيزياء على ما قدموه من علم ودعم وتشجيع طوال سنوات الدراسة، وإلى كل من أتاح لي فرصة الاستفادة من خبراته ومعارفه.

ولا يفوتني أن أعبر عن امتناني العميق لعائلتي الكريمة، وخاصة والدي ووالدتي، على ما قدماه من دعم معنوي وتشجيع دائم ودعاء صادق كان سندًا لي في جميع مراحل الدراسة والبحث. لهم مني كل الحب والتقدير.

وأتوجه أيضًا بالشكر إلى زملائي وأصدقائي الذين كانوا خير معين لي، سواء بالنقاشات العلمية أو تبادل الأفكار أو الدعم النفسي خلال فترات العمل الجاد.

ولا أنسى أن أشكر كل من ساهم بأي شكل من الأشكال في تسهيل إنجاز هذا البحث، سواء بالمعلومات أو التسهيلات أو المشورة، ولكل من وقف معي بكلمة طيبة أو دعوة صادقة.

أسأل الله أن يكتب للجميع الأجر والمثوبة، وأن يوفقنا جميعًا لما يحبه و يرضاه.

.

Table of Contents

List of Tables

List of Figures

الملخص

في هذه الدراسة، تم دراسة تأثير المجالات المغناطيسية على مسارات حزمة البروتونات لعلاج الأورام باستخدام محاكاة Geant4 ,تم محاكاة تفاعلات البروتونات عند مواضع الأورام السطحية والمتوسطة والعميقة لتحليل ترسيب الطاقة. تم تحليل الطاقة المترسبة في مناطق ما قبل الورم، والورم، وما بعد الورم لتحديد معايير العلاج المثلى. كشفت النتائج عن علاقة معقدة وغير خطية بين طاقة حزمة البروتون وشدة المجال المغناطيسي فيما يتعلق بنسبة الطاقة المترسبة في منطقة الورم. وتسلط هذه النتائج الضوء على أهمية الضبط الدقيق لكل من طاقة البروتون ومعايير المجال المغناطيسي لتعزيز دقة العلاج وفعاليته.

Abstract

In this study, the impact of magnetic fields on proton beam trajectories for tumor treatment was investigated using Geant4 simulations. Proton interactions were simulated at shallow, medium, and deep tumor positions to assess energy deposition. The energy deposited in the pre-tumor, tumor, and post-tumor regions was analyzed to determine the optimal treatment parameters. Results reveal a complex, non-linear relationship between proton beam energy and magnetic field strength in relation to the percentage of energy deposited in the tumor region. These findings highlight the importance of carefully tuning both proton energy and magnetic field parameters to enhance treatment precision and effectiveness.

.

Chapter 1: Introduction

1.1 Proton beam radiation therapy

The therapeutic potential of proton depth-dose characteristics was initially recognized in a report by Wilson in 1946, wherein he theorized the application of proton beams for the treatment of localized cancers. Within a decade, the first patient was treated using protons in 1954 at the University of California, Berkeley, employing the synchrocyclotron. Between this time and approximately 1990, several research accelerators globally were adapted for proton therapy, with the Harvard Cyclotron Laboratory (HCL) in Cambridge, Massachusetts, being particularly notable. Under the leadership of Suit and Goitein, HCL initiated a proton therapy program in 1973 targeting multiple cancer sites. Additionally, significant patient treatments were conducted at Uppsala University in Sweden, Dubna in Russia, and Chiba in Japan. When protons of specific energies (typically ranging from 70 to 250 MeV) penetrate matter, they decelerate continuously as a function of depth, with their energy loss, referred to as linear energy transfer (LET), increasing as their velocity decreases until they abruptly stop. This process results in a characteristic depth-dose curve known as the Bragg curve, with the maximum dose point designated as the Bragg peak. The depth of this peak, or the range of protons, is contingent upon the initial energy, with negligible dose deposition occurring beyond this range. Proton beam radiation therapy has evolved into a well-established treatment modality for various tumor types and sites, demonstrating advantages over photon therapy in terms of tumor control probability and reduced complications to normal tissues. Numerous dosimetric studies have consistently shown superior sparing of normal tissues with protons, particularly for tumors located in proximity to critical structures, such as in head-and-neck treatments; however, there are specific circumstances where the advantages may be marginal.

The primary rationale for the use of proton therapy is its exquisite physical dose deposition characteristics. Expectations have been that such dose distributions will allow significant sparing of normal tissues adjacent to the target volume or target dose escalation, or both [1, 2, 3, 4]

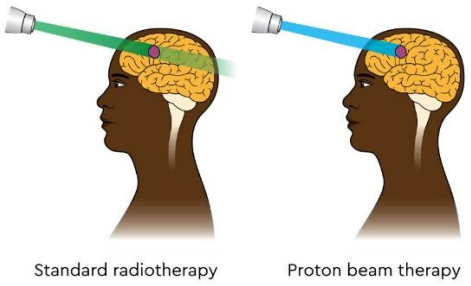

Figure 1.1: Standard radiotherapy and proton beam therapy. [5]

1.1.1 Advantages of proton beam therapy

- Proton therapy stands out for its precise control of radiation dose distribution, primarily due to the Bragg Peak phenomenon, which allows protons to deposit maximum energy at a specific depth within the tumor while minimizing exposure to surrounding healthy tissues. This unique physical property makes proton therapy particularly effective for targeting complex tumors, especially those located near critical structures such as skull base tumors and head-and-neck malignancies, where dose reduction to sensitive tissues is crucial. Additionally, advanced radiation scanning techniques like Pencil Beam Scanning (PBS) enable highly precise dose modulation, allowing adaptive dose shaping that conforms to the tumor's geometry, thereby enhancing treatment efficacy while further reducing radiation exposure to healthy tissues. [1, 2]

- Proton therapy offers a significant reduction in total body radiation dose, This minimizes radiation exposure to healthy tissues and lowers the risk of long-term radiation toxicity, which is particularly vital for pediatric patients, as reducing radiation to developing organs improves post-treatment quality of life. Additionally, proton therapy helps mitigate side effects in pediatric and radiation-sensitive patients by reducing the risk of neurocognitive impairments and minimizing adverse effects on bone and tissue development, making it a preferred option for young patients requiring radiation treatment. Moreover, the lower cumulative radiation dose in proton therapy significantly decreases the risk of secondary malignancies caused by unnecessary

radiation exposure, offering a crucial advantage over conventional photon therapy, especially for patients requiring long-term radiation treatment. [2]

1.2 Proton interactions with matter

When a proton passes through matter, it undergoes three distinct types of interactions: collisions with atomic electrons, and nuclear interactions.

Inelastic Coulomb interactions occur when a proton collides with an atomic electron, causing the proton to lose energy through ionization and excitation of the electron.

Elastic Coulomb interactions involve the proton interacting with an atomic nucleus. Due to the repulsive Coulomb force between the positively charged proton and nucleus, the proton is elastically scattered or deflected without significant energy loss.

Nuclear interactions happen when a high-energy proton collides directly with an atomic nucleus. This can result in a non-elastic collision that produces secondary particles from within the nucleus.[6]

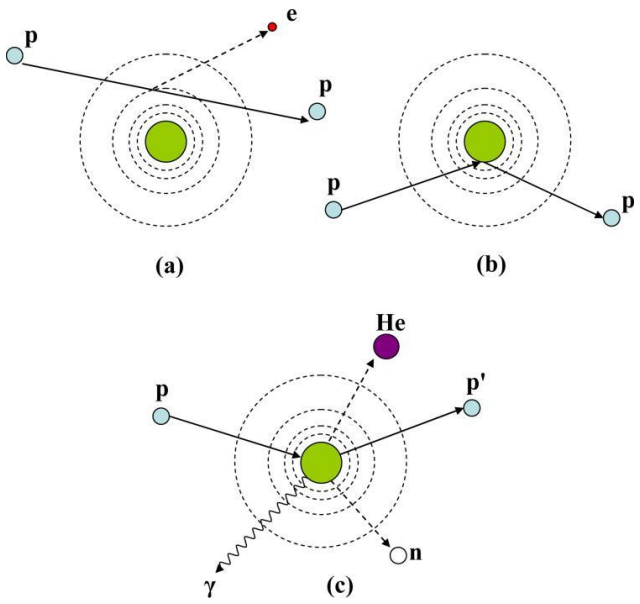

Figure 1.2: Proton interactions with matter. (a) proton interactions with electron , (b) elastic scattering proton with nucleus , (c) proton interactions with nucleus [6]

These interactions determine the shape of the Bragg peak, which represents the depth-dose distribution of protons. In other words, the Bragg peak refers to the point at which protons deposit their maximum energy. This characteristic is the main advantage of proton therapy, as it allows for precise dose delivery to the target tissue while minimizing damage to surrounding healthy tissue.[7]

1.3 Impact of magnetic field in proton therapy

Charged particles generally travel in a straight line. However, when a beam of protons passes through a magnetic field, it experiences a deflection due to the Lorentz force. This force causes the protons to follow a circular trajectory within the magnetic field. There is an relationship between the strength of the magnetic field and the angle of deflection. [8]

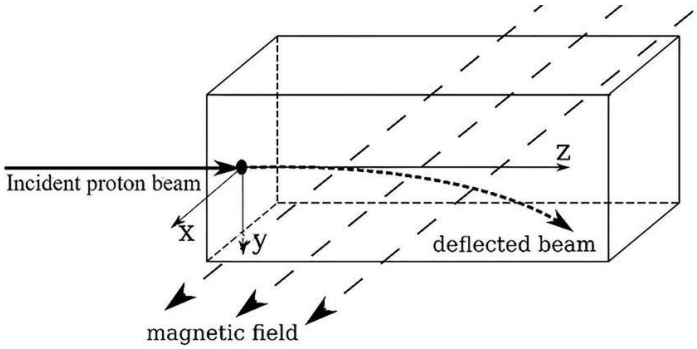

Figure 1.3: Deflection of proton beam within magnetic field. [9]

Magnetic fields can be utilized to precisely deliver radiation doses to targeted tumors while minimizing exposure to healthy tissues. By redirecting the proton beam and regulating its penetration depth, the magnetic field helps optimize treatment effectiveness based on the relationship between the beam's radius of curvature and the magnetic field strength. [10]

1.4 Geant4

In cases involving cancer patients, it is essential to develop a comprehensive treatment plan that incorporates imaging techniques to accurately determine the location and size of the tumor. Simulation plays a critical role in this process, as it enables the precise calculation of the energy levels and the trajectory that the electron beam must follow. This ensures effective tumor treatment while minimizing damage to the surrounding healthy tissues.

Geant4 is a toolkit for simulating the passage of particles through matter. It includes a complete range of functionality including geometry, tracking, and physics models. The physics processes offered cover a comprehensive range, including electromagnetic, hadronic and optical processes, a large set of long-lived particles, materials and elements, over a wide energy range starting, in some

cases, from and extending in others to the TeV energy range. It has been designed and constructed to expose the physics models utilised, to handle complex geometries, and to enable its easy adaptation for optimal use in different sets of applications. The toolkit is the result of a worldwide collaboration of physicists and engineers. It has been created exploiting software engineering and object-oriented software technology and implemented in the C++ programming language. It has been used in applications in particle physics, nuclear physics, accelerator design, space engineering and medical physics [11]

.

1.5 Aim of this work

This study aims to investigate the impact of a magnetic field on proton beams to enhance the effectiveness of proton therapy. This involves analyzing how magnetic field affects the tumor energy deposit. By performing energy deposition analysis across the pre-tumor, tumor, and post-tumor regions, the optimal treatment configuration can be determined.

Chapter 2: Materials & Methods

2.1 Simulation

GEANT4 is an open-source software toolkit designed for simulating the interaction of particles with matter. It is developed in C++ using object-oriented programming principles. GEANT4 is widely used in various fields such as nuclear particle physics, accelerator design, nuclear medicine, and space science. The system is structured around key modules that enable comprehensive, high-fidelity simulations for particle-matter interactions. The Geometry module allows precise definition of complex structures and materials through Constructive Solid Geometry (CSG) and Boundary Representations (BREPs), while the Physics module supports a wide range of physical processes including electromagnetic, hadronic, decay, and optical interactions such as Cherenkov radiation and scintillation. Particle tracking is performed step-by-step, taking into account magnetic fields and geometric boundaries,and event management efficiently handles both primary and secondary events, including pile-up scenarios common in high-intensity environments. The system offers high flexibility through abstract interfaces that allow customization and extension of physics models, and supports a broad energy range from 250 eV to several TeV. Efficiency is enhanced via optimized navigation algorithms such as smart voxels and fast simulation (parameterization) techniques that reduce computational overhead in scenarios like electromagnetic or hadronic shower development. The physics models include detailed electromagnetic processes (e.g., electron ionization, Bremsstrahlung,and multiple scattering), low-energy interactions down to 250 eV, and hadronic interactions modeled using evaluated nuclear data libraries (e.g., ENDF/B) and theoretical frameworks such as the dual parton model.Optical processes are also supported, including photon reflection,refraction, absorption, Cherenkov emission, and scintillation. For visualization and analysis, the system integrates with rendering tools like DAWN and VRML for high-quality graphical output and geometry validation and supports interactive exploration of geometries and particle trajectories. Data analysis is facilitated through interfaces such as AIDA, enabling compatibility with external tools like JAS and Lizard. Developed collaboratively by an international network of laboratories and academic institutions, the system is regularly updated and has found wide application across multiple domains including particle physics (e.g., LHC detector

simulations), nuclear medicine (e.g., proton therapy dose calculations), and space science (e.g., modeling cosmic radiation effects on spacecraft). [11]

2.2 Work process phases

2.2.1 Phase one: Validation of the Geant4 simulation

In this phase, the study will focus on setting up a simulation system using Geant4, where a uniform magnetic field is applied in the positive y-direction in air. Proton beams of specific energies are generated and sent in the negative z-direction perpendicular to the magnetic field. The deflection angle of proton beams will be calculated both manually and using Geant4. The manually calculated angles will be based on theoretical formulas, and the results will be compared to the simulated deflection angles to validate the Geant4 simulation code. The error percentage between the simulated and manually calculated angles will be computed to assess the accuracy of the Geant4 simulation.

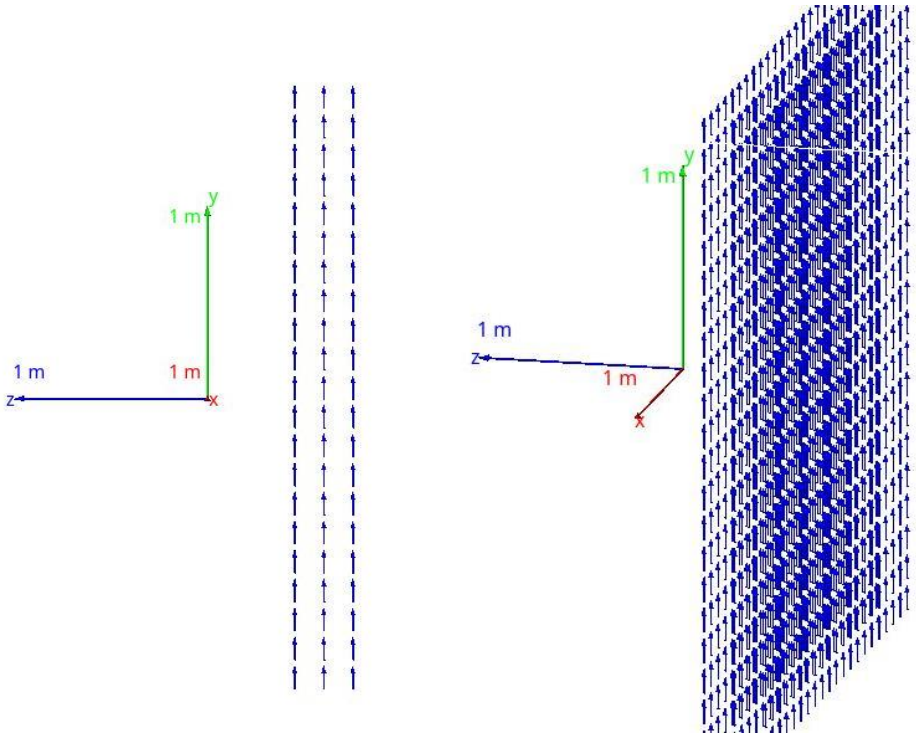

Figure 2.1: Direction of magentic field in the Geant4 simulation code.

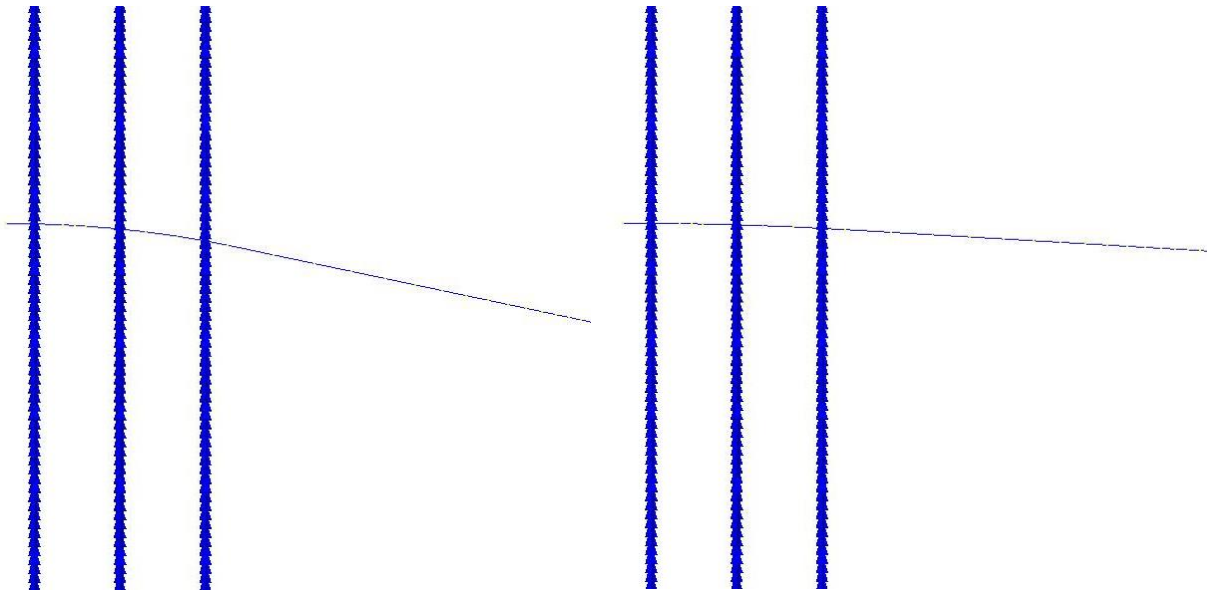

Figure 2.2: Proton beam trajectory in different magnetic fields.

2.2.2 Phase two: Adding a water phantom and a tumor

This phase relies on phase one by introducing a water phantom to simulate tissue interactions. A tumor, modeled with a tissue similar material with a density greater than that of water (G4_TISSUE_SOFT_ICRP), will be placed at shallow, medium, and deep positions within the phantom. The proton trajectories will be simulated for various tumor positions and proton energies. The energy deposition within the tumor will be calculated.

The effectiveness of proton therapy will be evaluated by measuring the energy deposition in the pre-tumor, tumor, and post-tumor regions at different proton energies an different magnetic fields ensuring the targeted dose is delivered to the tumor while minimizing damage to healthy tissues.

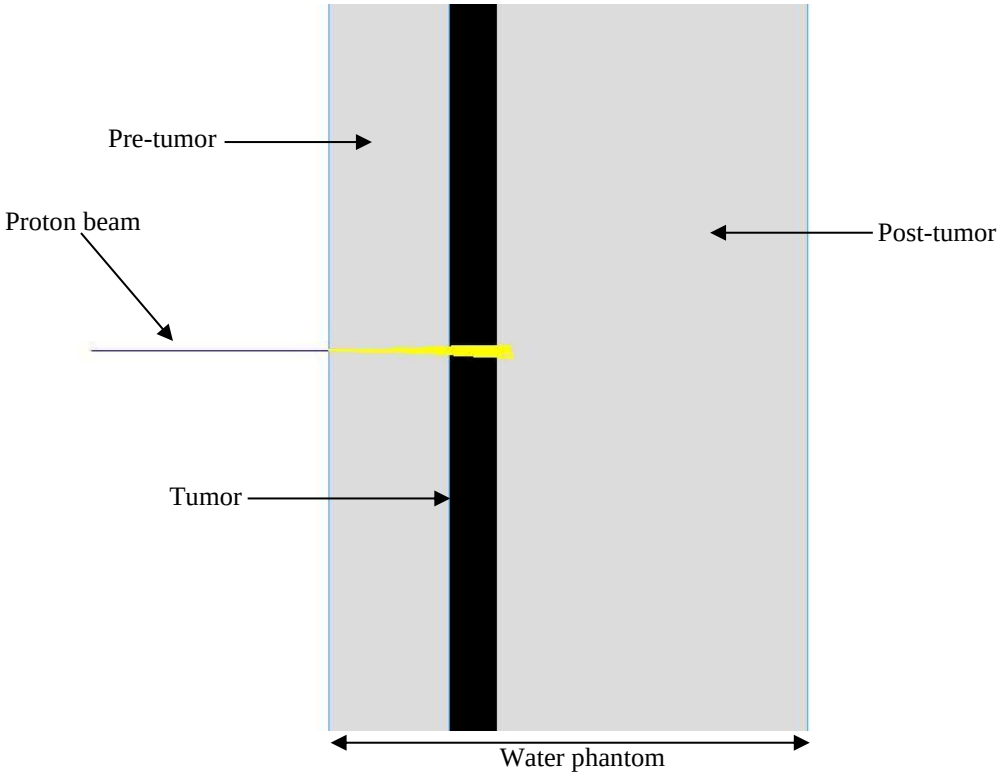

Figure 2.3: Proton beam passing through the water phantom with a magnetic field applied.

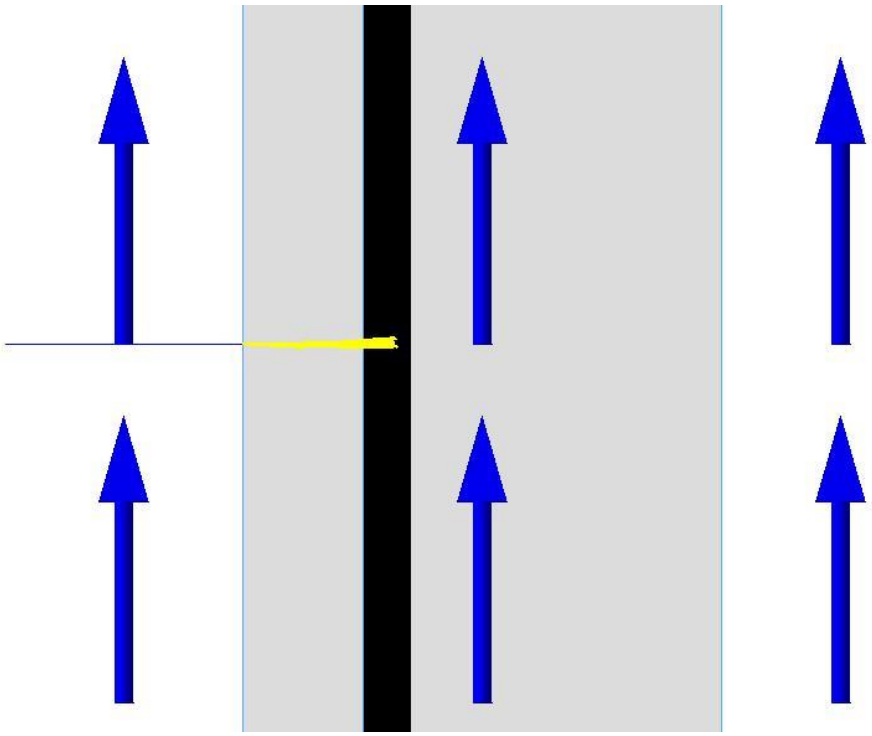

Figure 2.4: Proton beam passing through the water phantom showing the direction of magnetic field applied.

2.3 Mathematical Framework

2.3.1 : Angle found by Geant4

In the Geant4 code, the principle of momentum conservation was applied using the initial momentum of a charged particle before it enters the magnetic field, and the final momentum after it exits in order to find the angle of deflection. Then, the angle of deflection was determined by computing the dot product of the two momentum vectors: [12]

$$\cos\theta = \frac{\overrightarrow{p_i} \cdot \overrightarrow{p_f}}{|\overrightarrow{p_i}| \cdot |\overrightarrow{p_f}|} \qquad (2.1)$$

2.3.2 Angle found by Lorentz force

According to Newton's second law, if the net force acting on an object is zero, its acceleration is also zero. This means its velocity remains constant, and it will continue to move in a straight line. This explains why charged particles travel in straight paths when no external forces act on them. However, when a charged particle enters a magnetic field, it experiences a magnetic force known as the "Lorentz force" which will be described by: [13]

$$\vec{F} = p(\vec{E} \times \vec{v} \times \vec{B}) \qquad (2.2)$$

If there no electric field:

$$\vec{F} = p(\vec{v} \times \vec{B}) \qquad (2.3)$$

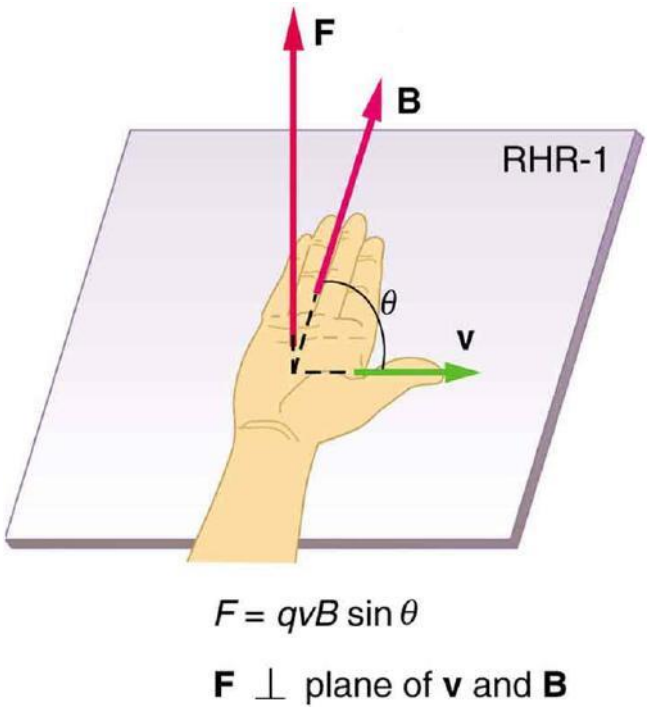

Figure 2.5: Right Hand Rule to determine the direction of magnetic force. [14]

The direction of this magnetic force is perpendicular to the plane formed by the velocity vector v and the magnetic field vector B, and it follows the right-hand rule–1 (RHR-1) as illustrated in Figure 2.5. The strength of the force is directly proportional to the charge p, the speed v, the magnetic field strength B, and the sine of the angle between the vectors v and B.

When velocity of charged particle perpendicular to magnetic field: [14]

$$F = p\ v\ B \qquad (2.4)$$

The Lorentz force is always perpendicular to the velocity of the particle, providing the necessary centripetal force that keeps the particle moving in a circular path. This perpendicular force causes the deflection of the particle's trajectory. Since the Lorentz force acts as the centripetal force, the equation becomes: [14]

$$p\ v\ B = m\frac{v^2}{r} \qquad (2.5)$$

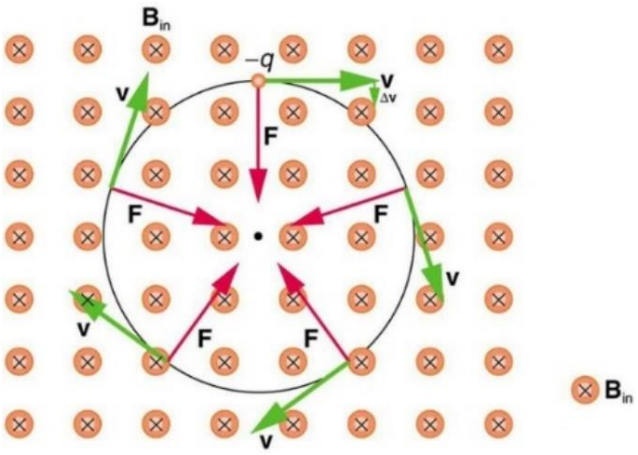

Figure 2.6: : Lorentz force suplise a centrepital force. [14]

The radius of circular motion described by: [14]

$$r = \frac{m\,v}{q\,B} \qquad (2.6)$$

Due to deflection of path the angle of defection can be found by measuring the length of the deflected path relative to the radius of the circular path: [15]

$$\theta = \frac{L}{r} = \frac{q\,B\,L}{m\,v} \qquad (2.7)$$

Where:

Is the angle of deflection θ

q is charge of particle

B is the magnitude of magnetic field

L is length of region of magnetic field

m is mass of particle

v is velocity of particle

Equation 2.7 was used to find the angle of deflection manually.

To determine the velocity of the particle, we employed the relativistic energy-momentum relationship, as we are dealing with subatomic particles—specifically, protons. In this context, relativistic effects become significant due to the high velocities involved. As a result, classical mechanics is insufficient for accurately describing their behavior. Therefore, we use the following equation derived from special relativity: [16]

$$v = c\sqrt{1 - \left(\frac{mc^2}{E}\right)^2} \tag{2.8}$$

Where:

v is velocity of particle

c is speed of light

m is mass of particle

E is total energy

2.3.3 Validation of the Geant4 code

The purpose of Phase One is to ensure that the Geant4 code runs efficiently, calculates the angle of deflection both using Geant4 and manually, and computes the error percentage by comparing the simulated value with the theoretical or calculated value using the following relation:

$$Error\ percentage\ \% = \frac{simulated\ value - calculated\ value}{calculated\ value} \times 100$$

To validate the accuracy of the Geant4 code, we calculated the error percentage as shown below:

Table 2.1: calculation error percentage of deflection angle.

B (T)	E (MeV)	L (m)	v (m/s)	$\theta°$ (simulated)	$\theta°$ (calculated)	Error (%)
0.3	150	0.4	151987481	3.71621	4.33277	14.23
0.3	250	0.4	184082670	2.80938	3.57734	21.47
0.4	150	0.4	151987481	4.95718	5.77703	14.19
0.4	250	0.4	184082670	3.7468	4.76979	21.45
0.5	100	0.4	128383455	7.68735	8.55331	10.17
0.5	200	0.4	169759335	5.30209	6.46859	18.03
0.6	100	0.4	128383455	9.22019	10.2640	10.17
0.6	200	0.4	169759335	6.36581	7.76081	17.97

Based on the small error margin between the simulated angle and the calculated angle, we conclude that the Geant4 code results are efficient.

Chapter 3: Results

Proton therapy is considered one of the most advanced techniques in tumor treatment, as it allows the precise delivery of proton energy to the tumor, effectively destroying cancer cells while minimizing the impact on surrounding healthy tissues. Both the proton energy and the value of the magnetic field play a fundamental role in determining the energy distribution within the tumor mass. This study aims to analyze the relationship between proton energy, magnetic field, and the percentage of energy distributed within the tumor, with the goal of identifying the best combination to achieve higher therapeutic effectiveness.

3.1 Tumor at shallow position within the phantom

Proton therapy targeting a shallow tumor was simulated. Four magnetic field values were tested: 0.2, 0.4, 0.6, and 0.8 Tesla, with four proton beam energies for each case: 70, 72.5, 75, and 77.5 MeV. with thicknesses set at 2 cm pre-tumor, 2 cm within the tumor, and 16 cm post-tumor.

Due to the short distance between the beam entry point and the shallow tumor location, the deflection angle remained zero across all tested energy levels and magnetic field strengths. Furthermore, Notably the results showed that the highest energy deposited at the tumor site occurred at a magnetic field strength of 0.4 Tesla and a proton energy of 70 MeV, with a value of 133.633.

Table 3.1: Simulation results of treatment of a shallow tumor with a magnetic field of 0.2 Tesla.

B (T)	Proton Energy (MeV)	Energy Deposit (Pre-tumor)	Energy Deposit (Tumor)	Energy Deposit (Post-tumor)	Tumor energy deposit %
0.2	70	55.1374	133.601	0	70.78634
0.2	72.5	53.0976	103.631	39.8959	52.70503
0.2	75	51.0694	89.2413	62.9514	43.90454
0.2	77.5	49.7471	81.3611	78.6823	38.78207

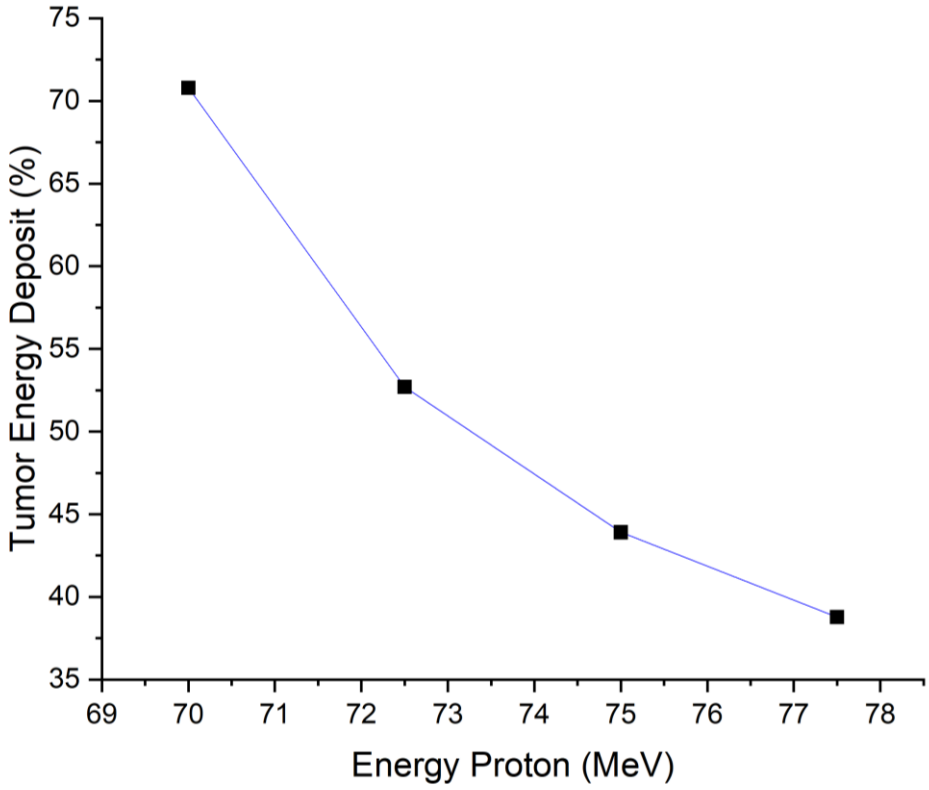

Figure 3.1: : Tumor energy deposit percentage at Magnetic field of 0.2 Tesla at different proton energies.

Table 3.2: Simulation results of treatment of a shallow tumor with a magnetic field of 0.4 Tesla.

B (T)	Proton Energy (MeV)	Energy Deposit (Pre-tumor)	Energy Deposit (Tumor)	Energy Deposit (Post-tumor)	Tumor energy deposit %
0.4	70	55.1404	133.633	0	70.79016
0.4	72.5	53.2693	104.058	39.9427	53.01778
0.4	75	51.1311	89.1186	63.1593	43.81252
0.4	77.5	49.8201	81.2288	78.2842	38.80361

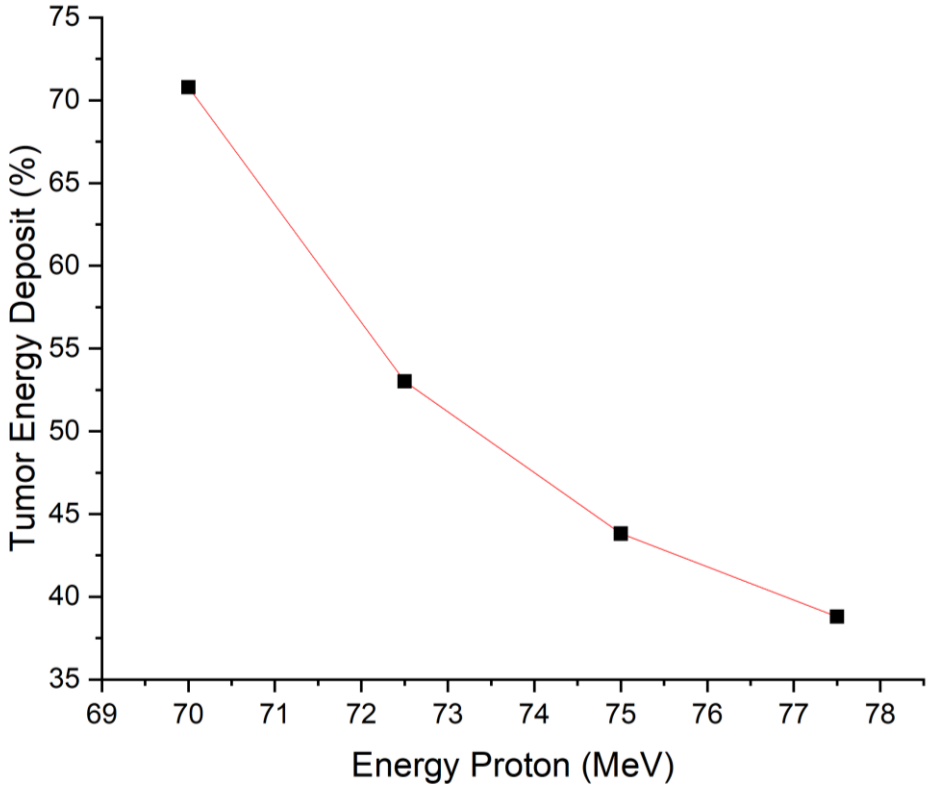

Figure 3.2: : Tumor energy deposit percentage at Magnetic field of 0.4Tesla at different proton energies.

Table 3.3: Simulation results of treatment of a shallow tumor with a magnetic field of 0.6 Tesla.

B (T)	Proton Energy (MeV)	Energy Deposit (Pre-tumor)	Energy Deposit (Tumor)	Energy Deposit (Post-tumor)	Tumor energy deposit %
0.6	70	55.3283	133.449	0	70.69123
0.6	72.5	53.2053	104.495	38.5092	53.25685
0.6	75	51.1496	89.5381	62.9615	43.96683
0.6	77.5	49.9992	81.5209	78.411	38.83222

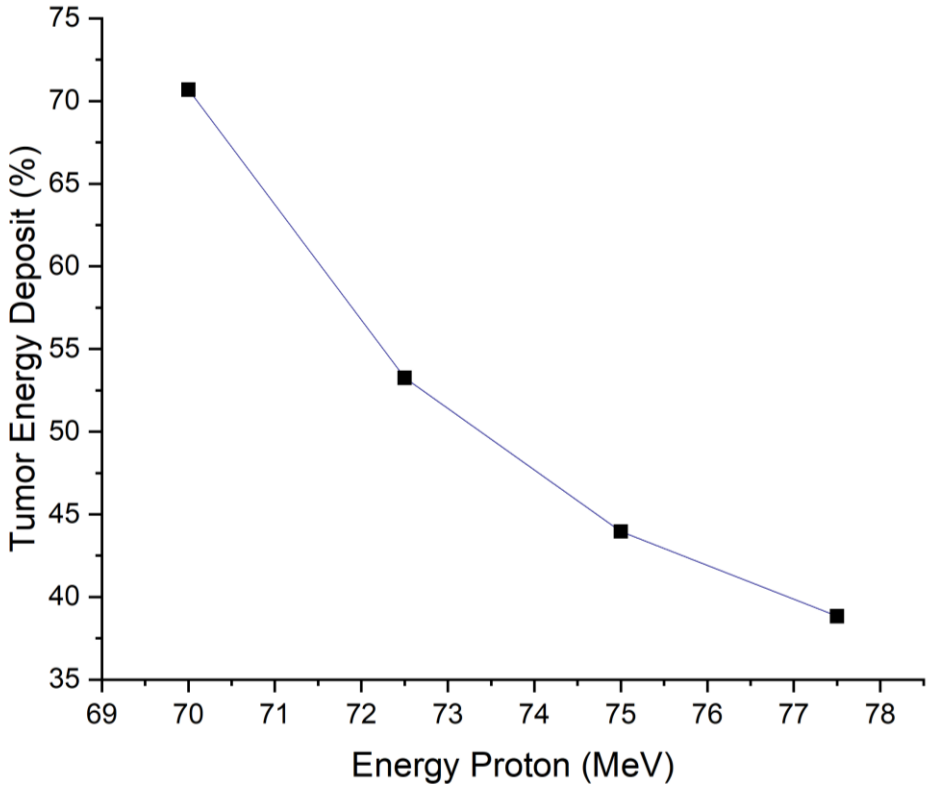

Figure 3.3: : Tumor energy deposit percentage at Magnetic field of 0.6 Tesla at different proton energies.

Table 3.4: Simulation results of treatment of a shallow tumor with a magnetic field of 0.8 Tesla.

B (T)	Proton Energy (MeV)	Energy Deposit (Pre-tumor)	Energy Deposit (Tumor)	Energy Deposit (Post-tumor)	Tumor energy deposit %
0.8	70	55.2026	133.355	0	70.72375
0.8	72.5	53.2775	105.158	37.9905	53.53568
0.8	75	51.018	89.7371	62.6025	44.12773
0.8	77.5	49.8777	82.063	78.4763	39.00018

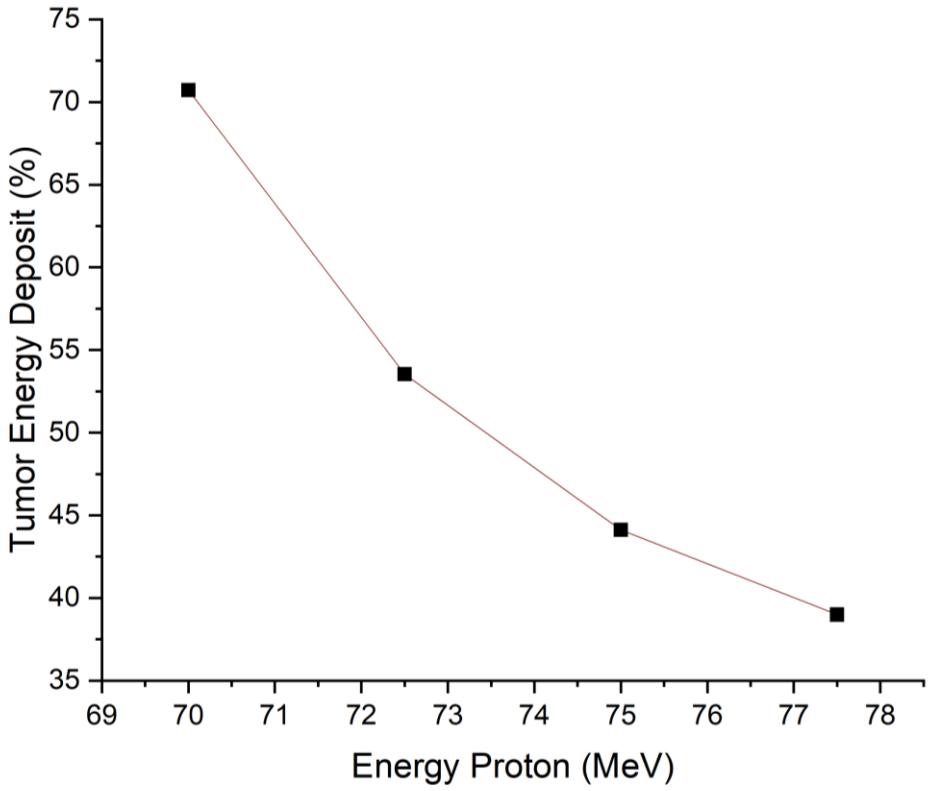

Figure 3.4: : Tumor energy deposit percentage at Magnetic field of 0.8 Tesla at different proton energies.

These results showed that the highest recorded percentage of tumor energy deposit, was 70.79016% of the total energy deposit.

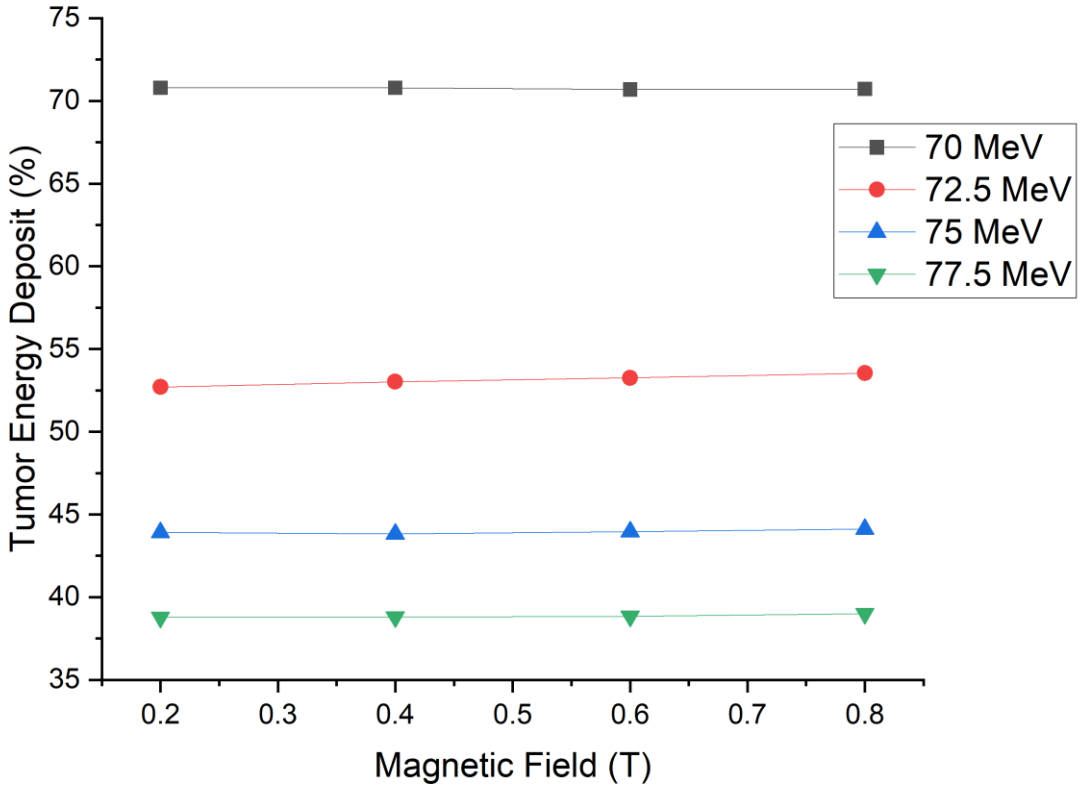

Figure 3.5: : Tumor energy deposit at proton energies of 70 , 72.5 , 75 and 77.5 MeV at different magnetic field.

The presented graph above illustrates the tumor energy deposition percentage as a function of magnetic field strength for fixed proton beam energies (70 MeV, 72.5 MeV, 75 MeV, and 77.5 MeV). Across all investigated magnetic fields, the tumor energy deposit remains essentially constant despite variations in the magnetic field from 0.2 T to 0.8 T. This indicates that, within the evaluated energy range, the magnetic field has a negligible impact on the energy delivered to the tumor. Therefore, for the specified energy values, magnetic field variations do not significantly alter the treatment dose distribution in the tumor region.

3.2 Tumor at medium position within the phantom

To investigate the impact of energy and magnetic field strength on treatment efficiency, protons with varying energies (94, 94.5, 95, and 95.5 MeV) were emitted under specific magnetic field strengths (0.8, 1, 2, 3, and 4 T), with thicknesses set at 5 cm pre-tumor, 2 cm within the tumor, and 13 cm post-tumor.

Table 3.5: Simulation results of treatment of a mid-depth tumor with a magnetic field of 0.8 Tesla.

B (T)	Proton Energy (MeV)	Energy Deposit (Pre-tumor)	Energy Deposit (Tumor)	Energy Deposit (Post-tumor)	Tumor energy deposit %
0.8	94	122.484	127.58	0	51.01894
0.8	94.5	122.441	129.42	0	51.38549
0.8	95	120.274	128.12	4.3892	50.68375
0.8	95.5	119.864	128.259	5.96136	50.4789

Table 3.6: Simulation results of treatment of a mid-depth tumor with a magnetic field of 1 Tesla.

B (T)	Proton Energy (MeV)	Energy Deposit (Pre-tumor)	Energy Deposit (Tumor)	Energy Deposit (Post-tumor)	Tumor energy deposit %
1	94	122.577	127.487	0	50.98175
1	94.5	122.37	129.119	0	51.34181
1	95	120.991	128.046	3.80826	50.64204
1	95.5	120.112	128.456	5.57201	50.54537

Table 3.7: Simulation results of treatment of a mid-depth tumor with a magnetic field of 2 Tesla.

B (T)	Proton Energy (MeV)	Energy Deposit (Pre-tumor)	Energy Deposit (Tumor)	Energy Deposit (Post-tumor)	Tumor energy deposit %
2	94	124.637	125.54	0	50.18047
2	94.5	124.165	127.384	0	50.63984
2	95	120.825	130.214	4.57439	50.94178
2	95.5	122.051	130.37	1.30604	51.38199

Table 3.8: Simulation results of treatment of a mid-depth tumor with a magnetic field of 3 Tesla.

B (T)	Proton Energy (MeV)	Energy Deposit (Pre-tumor)	Energy Deposit (Tumor)	Energy Deposit (Post-tumor)	Tumor energy deposit %
3	94	128.099	121.445	0	48.66677
3	94.5	127.902	123.415	0	49.1073
3	95	126.346	126.022	0	49.93581
3	95.5	125.531	128.223	0	50.53043

Table 3.9: Simulation results of treatment of a mid-depth tumor with a magnetic field of 4 Tesla.

B (T)	Proton Energy (MeV)	Energy Deposit (Pre-tumor)	Energy Deposit (Tumor)	Energy Deposit (Post-tumor)	Tumor energy deposit %
4	94	115.503	115.503	0	46.04905
4	94.5	117.107	117.107	0	46.58491
4	95	119.81	119.81	0	47.54214
4	95.5	122.558	122.558	0	48.27057

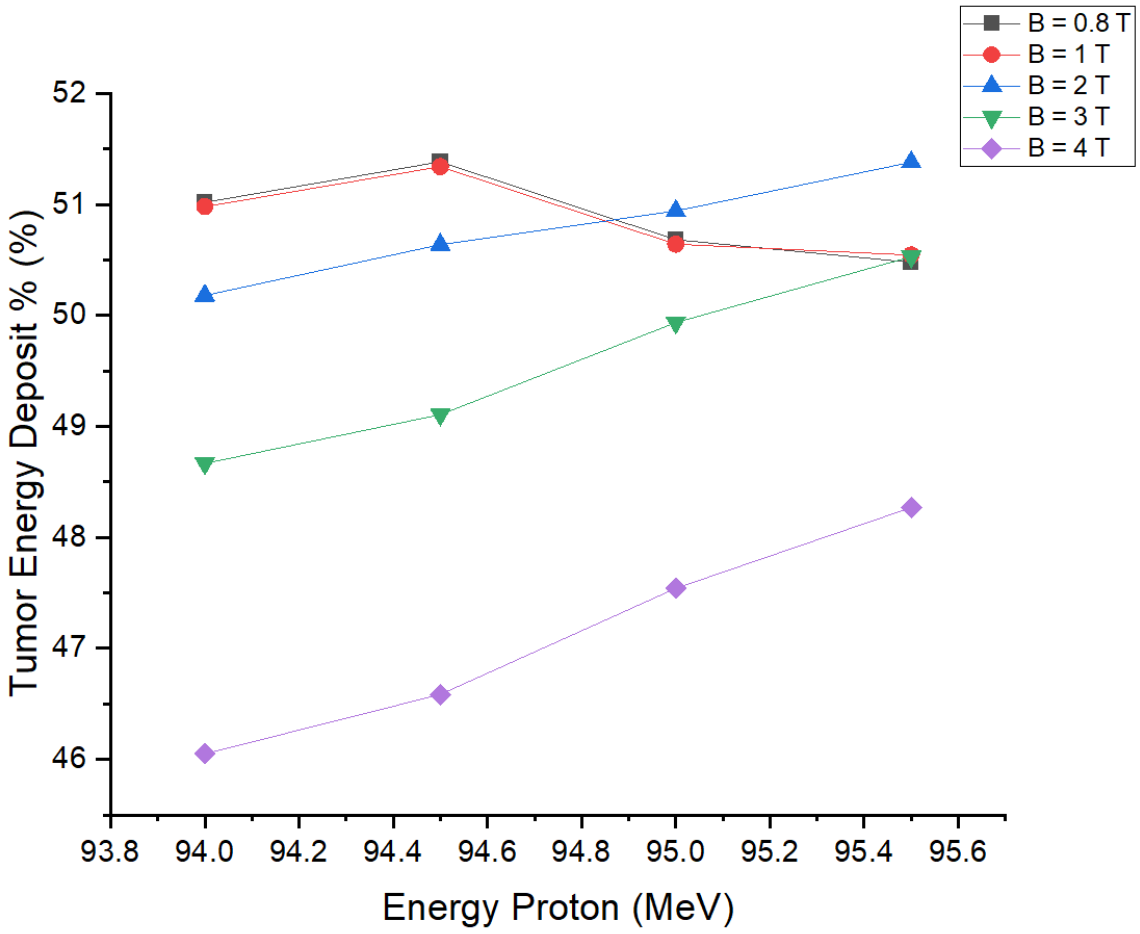

Figure 3.6: : Tumor energy deposit at magnetic field of 0.8 , 1 , 2 , 3 and 4 Tesla at different proton energies.

As shown in figure 3.6, the percentage of tumor energy deposit remains nearly constant across different magnetic field strengths. For example, at 0.8 T, the energy deposited in the tumor ranges slightly from 50.48 to 51.39 %. Similarly, at 1 T it ranges from 50.55 to 51.34%; at 2 T, from 50.18 to 51.38% ; at 3 T, from 48.67 to 50.53% ; and at 4 T, from 46.05 to 48.27% . This indicates that the magnetic field has minimal effect on the percentage of energy deposited in the tumor. The energy deposit post-tumor is observed to be zero , which indicates no damage to healthy tissues whereas increasing the proton energy causes a slight shift in the Bragg peak. Notably, at 95 MeV, a higher amount of energy is deposited beyond the tumor region, potentially causing damage to healthy tissues. Therefore, it is crucial to carefully control the proton energy to ensure that the maximum energy is deposited within the tumor region.

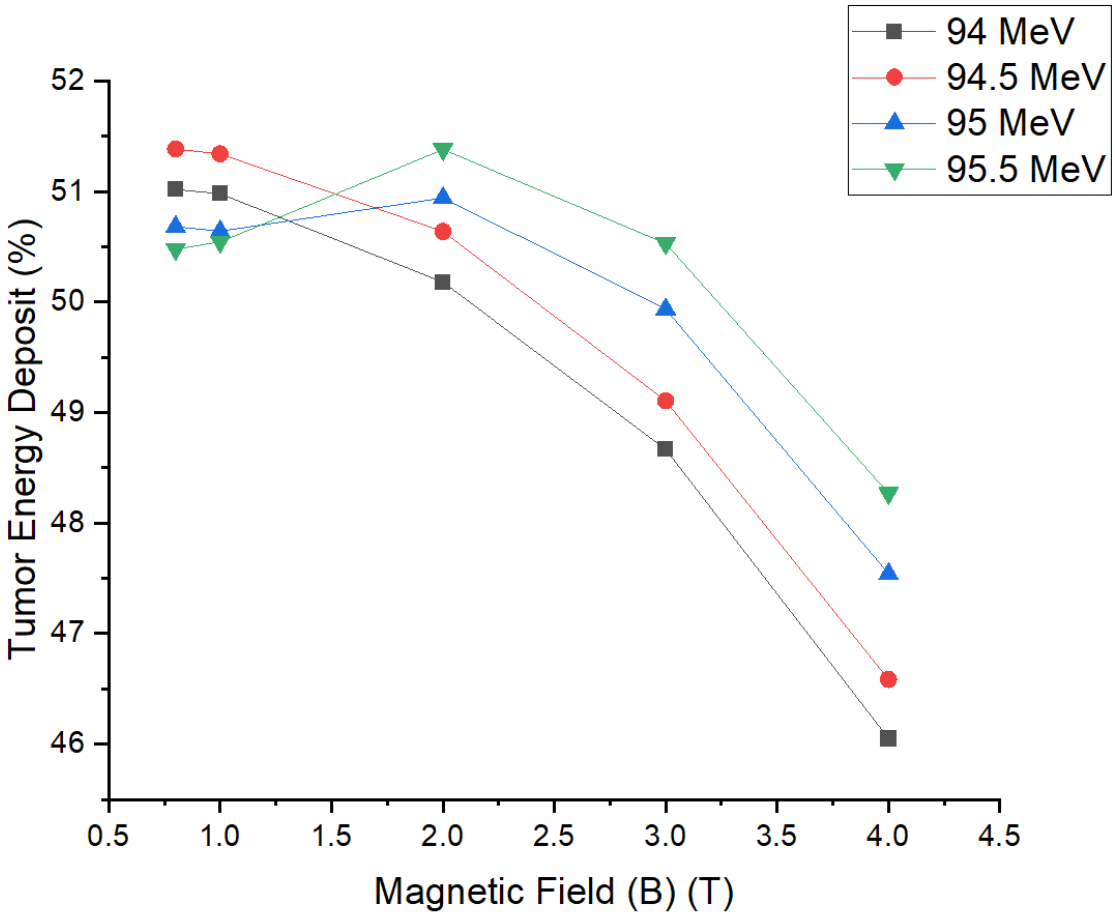

Figure 3.7: Tumor energy deposit at proton energies of 94 , 94.5 , 95 and 95.5 MeV at different magnetic field.

According to the figure, the magnetic field has a significantly greater effect on tumor energy deposition compared to proton energy. The graph shows that as the magnetic field strength increases; the percentage of energy deposited in the tumor decreases. For example, at a proton energy of 94 MeV, the tumor energy deposition drops from 51.01% to 46.05% as the magnetic field strength increases from 0.8 T to 4 T (specifically: 51.01%, 50.98%, 50.18%, 48.67%, and 46.05% at 0.8, 1, 2, 3, and 4 T, respectively). This reduction is attributed to the Lorentz force, which causes the protons to deviate from their intended path. As the magnetic field increases, this deflection becomes more pronounced, reducing the precision of proton beam delivery to the tumor site and thereby decreasing the effectiveness of the treatment.

3.3 Tumor at deep position within the phantom

The energy distribution within the tumor was simulated using four different magnetic field values (0.2 T, 0.4, 0.6 T, 1.2 T) at three proton energy levels (115.0 MeV, 115.5 MeV, 116.0 MeV). with thicknesses set at 8 cm pre-tumor, 2 cm within the tumor, and 10 cm post-tumor.

The percentage of energy deposited within the tumor (Tumor %) was measured for each case, as illustrated in the following table and graph.

Table 3.10: Simulation results of treatment of a deep tumor with a magnetic field of 0.2 Tesla.

B (T)	Proton Energy (MeV)	Energy Deposit (Pre-tumor)	Energy Deposit (Tumor)	Energy Deposit (Post-tumor)	Tumor energy deposit %
0.2	115	178.314	125.486	0	41.30546412
0.2	115.5	179.4	126.588	126.588	41.5779425
0.2	116	175.152	126.44	4.5179	41.30542658

Table 3.11: Simulation results of treatment of a deep tumor with a magnetic field of 0.4 Tesla.

B (T)	Proton Energy (MeV)	Energy Deposit (Pre-tumor)	Energy Deposit (Tumor)	Energy Deposit (Post-tumor)	Tumor energy deposit %
0.4	115	178.46	125.292	0.0222379	41.24508473
0.4	115.5	176.649	126.798	01.2937	41.60848879
0.4	116	175.349	126.496	4.10451	41.34538408

Table 3.12: Simulation results of treatment of a deep tumor with a magnetic field of 0.6 Tesla.

B (T)	Proton Energy (MeV)	Energy Deposit (Pre-tumor)	Energy Deposit (Tumor)	Energy Deposit (Post-tumor)	Tumor energy deposit %
0.6	115	125.534	125.534	0	41.34045097
0.6	115.5	126.829	126.829	0.751428	41.7524007
0.6	116	175.975	127.144	3.19572	41.50763633

Table 3.13: Simulation results of treatment of a deep tumor with a magnetic field of 1.2 Tesla.

B (T)	Proton Energy (MeV)	Energy Deposit (Pre-tumor)	Energy Deposit (Tumor)	Energy Deposit (Post-tumor)	Tumor energy deposit %
1.2	115	178.314	125.362	0	41.28149739
1.2	115.5	177.443	126.761	0	41.66973478
1.2	116	176.781	128.833	0.491718	42.08774695

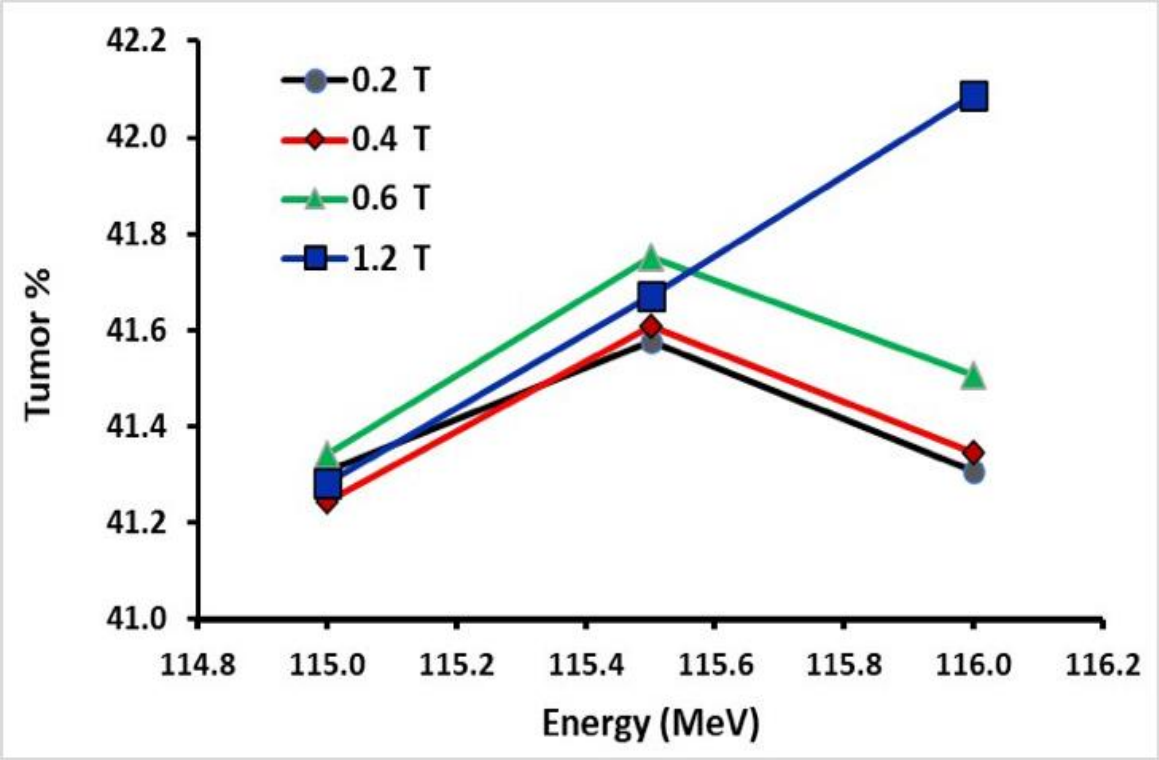

Figure 3.8: Tumor energy deposit at magnetic field of 0,2 , 0.4 , 0.6 and 1.2 Tesla at different proton energies.

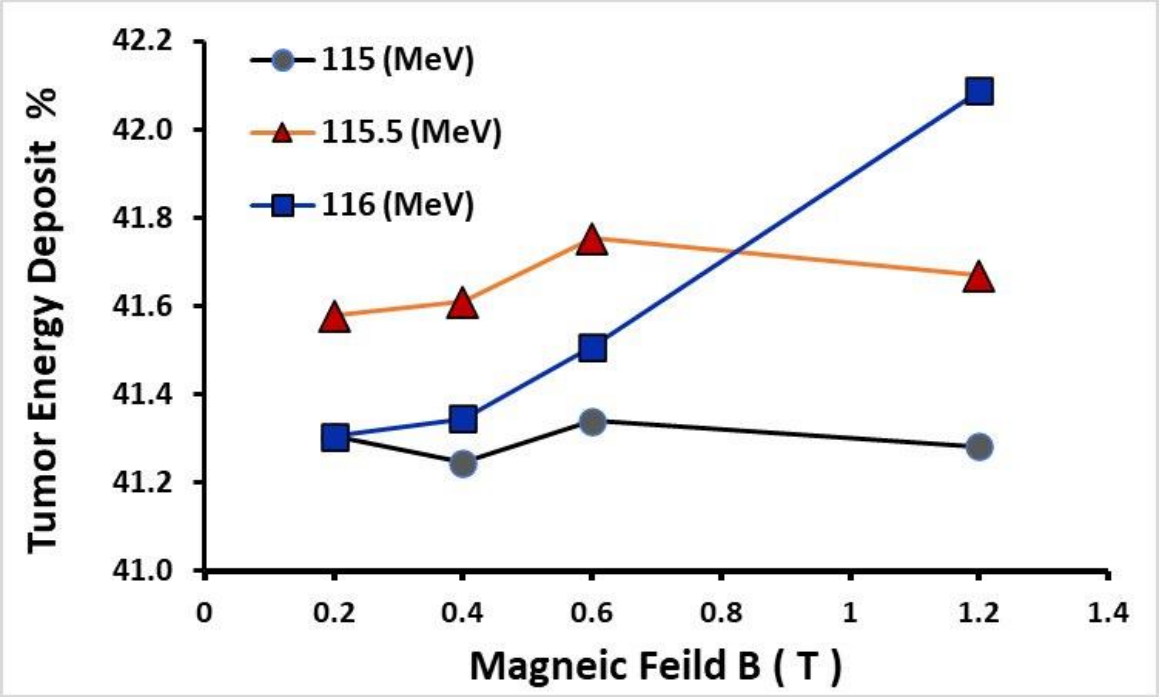

Figure 3.9: Tumor energy deposit at proton energies of 115 , 115.5 and 116 MeV at different magnetic field.

At Proton Energy of 115.0 MeV, all values for the magnetic field are very close (41.2–41.3%). This indicates that the effect of the magnetic field is almost negligible at this relatively low energy On the other hand, at proton energy of 115.5 MeV; a relative increase in the percentage of energy within the tumor was observed for all magnetic field values

The 0.6 T magnetic field showed a slight advantage (41.7%) compared to the other values (41.6%) This suggests that there is an optimal range of energy and magnetic field that can be utilized to enhance treatment effectiveness at proton energy of 116.0 MeV

The high magnetic field (1.2 T) recorded the highest energy distribution percentage within the tumor (42.2%), which is a noticeable difference from the other values.

The remaining values (0.2 T, 0.4 T, 0.6 T) yielded lower percentages (41.3–41.5%) relationship between variables The relationship between proton energy and increasing magnetic field is not entirely linear rather there are mutual effects that depend on the value of each variable At lower energies, the effect of the magnetic field is limited, while at higher energies, its influence becomes evident at a proton energy of 116.0 MeV and a magnetic field of 1.2 T the highest energy distribution within the tumor can be achieved, enhancing the effectiveness of proton therapy

If a high magnetic field is not available a 0.6 T magnetic field with a proton energy of 115.5 MeV can be a good alternative. The effect of the magnetic field increases with rising proton energy confirming the importance of studying the interaction between these two variables to achieve optimal therapeutic outcomes.

Chapter 4: Discussion

This chapter presents the outcomes of the study, which aimed to investigate the effect of magnetic field strength and proton energy on the energy distribution within a tumor during proton therapy using Geant4 simulations. The experiments were divided into three main scenarios based on the tumor's location within the water phantom: shallow, medium, and deep. Each scenario explored different combinations of proton energies and magnetic field intensities to determine the optimal conditions for maximizing energy deposition in the tumor

For the shallow tumor position, the results revealed that varying the magnetic field from 0.2 to 0.8 Tesla, while using fixed proton energies of 70, 72.5, 75, and 77.5 MeV, had a negligible effect on the percentage of energy deposited in the tumor. The energy deposition remained nearly constant across all tested magnetic fields. The best result was observed at a magnetic field strength of 0.4 Tesla and a proton energy of 70 MeV, where the tumor received up to 70.79% of the total deposited energy, marking the highest value among the studied cases. This suggests that for shallow tumors, low to moderate magnetic fields with lower proton energies can achieve the highest therapeutic effectiveness without significant loss due to magnetic deflection.

When the tumor was positioned at a medium depth, the study considered a wider range of magnetic fields (0.8, 1, 2, 3, and 4 Tesla) and proton energies (94, 94.5, 95, and 95.5 MeV). It was found that increasing the magnetic field strength led to a gradual decrease in the percentage of energy deposited in the tumor. For instance, at a proton energy of 94 MeV, the energy deposition dropped from 51.01% at 0.8 Tesla to 46.05% at 4 Tesla. This reduction is attributed to the Lorentz force, which causes more pronounced deflection of the proton beam as the magnetic field increases, resulting in decreased precision in delivering the dose to the tumor. Therefore, for medium-depth tumors, it becomes essential to carefully control both the proton energy and the magnetic field to maintain treatment accuracy and avoid unnecessary irradiation of healthy tissues.

For tumors located at deeper positions within the phantom, the simulations tested magnetic fields from 0.2 to 1.2 Tesla and proton energies of 115, 115.5, and 116 MeV. The results indicated that at lower proton energies, the magnetic field had a limited impact on the energy deposited in the tumor. However, as the proton energy increased, the influence of the magnetic field became more noticeable. The highest energy deposition in the tumor, 42.09%, was achieved at a proton energy

of 116 MeV and a magnetic field of 1.2 Tesla, suggesting that high proton energies combined with stronger magnetic fields can improve the dose delivered to deep-seated tumors.

In summary, the relationship between proton energy and magnetic field strength is complex and non-linear, and it varies depending on the tumor's location and characteristics. The study emphasizes the importance of optimizing both variables to achieve the best possible therapeutic outcomes while minimizing the risk to surrounding healthy tissue. These findings highlight that for shallow tumors, lower proton energies and moderate magnetic fields are most effective, while for medium and deep tumors, careful balancing of both parameters is required to maximize energy deposition within the tumor and enhance the effectiveness of proton therapy.

References

[1] PAGANETTI, Harald. Proton beam therapy. Bristol: IOP Publishing, 2017.

[2] Proton Therapy Physics

Editor:Harald PaganettiPublisher:CRC PressYear:2018Edition:2

http://dx.doi.org/10.1201/b22053

[3] Proton therapy – Present and future

Authors:Radhe Mohan, David GrosshansJournal:Advanced Drug Delivery

ReviewsVolume:109Year:2017Pages:26—44

http://dx.doi.org/10.1016/j.addr.2016.11.006

[4]A review of proton therapy – Current status and future directions

Mohan R. (2022). A Review of Proton Therapy - Current Status and Future Directions. Precision radiation oncology, 6(2), 164–176.

https://doi.org/10.1002/pro6.1149

[5] Proton beam therapy - Macmillan Cancer Support. (n.d.). Macmillan Cancer Support | The UK's leading cancer care charity.

https://www.macmillan.org.uk/cancer-information-and-support/treatment/types-of-treatment/radiotherapy/external-beam-radiotherapy/proton-beam-therapy

[6] The physics of proton therapy

Newhauser, W. D., & Zhang, R. (2015). The physics of proton therapy. Physics in Medicine and Biology, 60(8), R155—R209.

https://doi.org/10.1088/0031-9155/60/8/r155

[7] Paganetti, H. (Ed.). (2016). Proton Therapy Physics. CRC Press.

https://doi.org/10.1201/9780367803551

[8] Sanny, J., Moebs, W., & Ling, S. J. (2016). University Physics: Volume 2. 12th Media Services.

[9] Tahmasebi Birgani, M. J., Chegeni, N., Zabihzadeh, M., & Tahmasbi, M. (2017). Analytical investigation of magnetic field effects on Proton lateral deflection and penetrating depth in the water phantom: A relativistic approach. Electronic Physician, 9(12), 5932–5939.

https://doi.org/10.19082/5932

[10] Pham, T. T., Whelan, B., Oborn, B. M., Delaney, G. P., Vinod, S., Brighi, C., Barton, M., & Keall, P. (2022). Magnetic resonance imaging (MRI) guided proton therapy: A review of the clinical challenges, potential benefits and pathway to implementation. Radiotherapy and Oncology

https://doi.org/10.1016/j.radonc.2022.02.031

[11]Agostinelli, S., Allison, J., Amako, K., Apostolakis, J., Araujo, H., Arce, P., Asai, M., Axen, D., Banerjee, S., Barrand, G.,Behner, F., Bellagamba, L., Boudreau, J., Broglia, L., Brunengo, A., Burkhardt, H., Chauvie, S., Chuma, J., Chytracek, R., . . . Zschiesche, D. (2003). Geant4—a simulation toolkit. Nuclear

Instruments and Methods in Physics Research Section A: Accelerators, Spectrometers, Detectors and Associated Equipment, 506(3), 250–303.
https://doi.org/10.1016/s0168-9002(03)01368-8
[12] Pratiyogita Darpan. (2002, February). Competition Science Vision (Vol. 2, No. 22).
[13] David Halliday * Robert Resnick * Jearl Walker. (2014). Fundamentals of Physics - Extended 10th Edition. Wiley Custom Learning Solutions - USMA PH201/202 & PH251/252.
[14] Libretexts. (2018, September 3). 21.4: Motion of a charged particle in a magnetic field. Physics LibreTexts. https://phys.libretexts.org/Bookshelves/University_Physics/Physics_(Boundless)/21%3A_Magnetism/21.4%3A_Motion_of_a_Charged_Particle_in_a_Magnetic_Field
[15] Dewar, J. M., & Zill, D. G. (2011). Precalculus with Calculus Previews. Jones & Bartlett Learning, LLC.
[16] Libretexts. (2018b, October 4). 27.3: Relativistic Quantities. Physics LibreTexts. https://phys.libretexts.org/Bookshelves/University_Physics/Physics_(Boundless)/27:__Special_Relativity/27.3:_Relativistic_Quantities